

LATTICE RELAXATION IN SOLID SOLUTIONS: LONG-RANGE VS. SHORT-RANGE STRUCTURE AROUND Cr^{3+} AND Co^{2+} IN OXIDES AND SILICATES

MATTEO ARDIT

Dipartimento di Scienze della Terra, Università di Ferrara, Via Saragat 1, 44100 Ferrara, Italy

ABSTRACT

This work reports the results derived from the 3-year doctoral thesis project aimed at exploring some oxide and silicate structures as promising ceramic pigments with enhanced colorimetric properties with respect to the traditional colorants. Solid solutions of perovskite, aluminobite, and melilite compounds were obtained by doping octahedral and tetrahedral coordination sites with transition metal ions (e.g. Cr^{3+} , Co^{2+} , and Zn^{2+}) through a solid-state synthesis performed by means of an industrial-like process. The analytical techniques adopted to investigate the synthesized compounds allowed the determination of the “averaged” crystal structure, or the so termed *long-range* properties, and the *short-range* properties (i.e. the local structure around the substituting ions) through X-ray powder diffraction (XRPD) and electronic absorption spectroscopy (EAS), respectively. As stated by Geiger (2001) “an understanding of the microscopic, mesoscopic and macroscopic properties and of the behaviour of solid solutions under different conditions is a challenge for all disciplines concerned with the solid state”. Hence, the precise determination of a structure around impurities results fundamental to provide detailed information on their incorporation and on physical properties. For instance, in the case of the solid solutions here reported, the lattice incorporation of transition metal ions as impurities is the cause of their gradual coloration. Most of the times, such a coloration is more intense as greater is the impurity amount.

The final goal of this work was attained by calculating the structural relaxation coefficient for each studied solid solution by combining the *mean* with the *local* bond distances achieved by XRPD and EAS, respectively.

INTRODUCTION

In an early application of X-ray diffraction to the analysis of crystal structure, Vegard (1921) observed that in many cubic ionic salts the lattice constant linearly scaled with the composition. This empirical rule, now known as “Vegard’s law”, has become accepted by many as of general validity, and employed in several scientific fields of mineralogy, metallurgy and materials science to extrapolate structural values in ideal binary solid solutions. Although Vegard’s law works well for many end-member compounds of isomorphous series, intermediate compositions within a solid solution series often display more complex behaviour. Deviations from this rule usually become as bigger as higher is the structural complexity of the examined systems.

The concept of structural relaxation

In the last decades, several experimental studies have demonstrated that the stability of isostructural solid solutions is affected, at the atomic scale, by a structural relaxation around substituting cations (e.g. Mikkelsen & Boyce, 1983; Urusov, 1992, 2001; Galois, 1996; Langer, 2001; Andrut *et al.*, 2004; Wildner *et al.*, 2004). Along a binary join, the information obtained by the “averaging” diffraction methods does not give any indication on the local distances between the central ion and its surrounding oxygen-based polyhedron. The lack of such an information may be overcome by the use of spectroscopic methods. As a matter of fact, structural data achieved through diffraction methods along a solid solution usually obeys Vegard’s rule, and both the lattice parameters and the average bond lengths might be found from the same additivity rule. For the hypothetical case of a $AO-BO$ solid solution, with mean bond lengths $\langle A-O \rangle$ and $\langle B-O \rangle$ for the A and B end-members, respectively, the Vegard’s rule applied to the bond distance of any intermediate term of composition $A_{1-x}B_xO$, will be:

$\langle A_{1-x}B_x-O \rangle = (1-x) \cdot \langle A-O \rangle + x \cdot \langle B-O \rangle$, where x is the amount of the replacing cation. As proposed by Urusov (1992), the deviation from Vegard's rule can be quantified, on a geometrical basis, through the relaxation coefficient (ε), as:

$$\varepsilon = (\langle B-O \rangle_x - \langle A-O \rangle) \cdot (\langle B-O \rangle - \langle A-O \rangle)^{-1} \quad (1)$$

where the mean polyhedral distances $\langle A-O \rangle$ and $\langle B-O \rangle$ are measured by diffraction methods, and $\langle B-O \rangle_x$ is the local mean distance for the sample $A_{1-x}B_xO$, with $x \rightarrow 0$ estimated by spectroscopy. From the latter equation emerges that the behaviour of exchanging cations in a solid solution falls between two extreme cases (see Fig. 1a). The assumption that all of the individual bond lengths in the mixed crystal are equal to their average values, $\langle B-O \rangle_x = \langle A-O \rangle$, implies that the relaxation is completely absent ($\varepsilon = 0$). Under another assumption, $\langle B-O \rangle_x = \langle B-O \rangle$, all the atoms in the solid solution preserve the initial size found in the doped end-member (Urusov, 1992, 2001; Wildner *et al.*, 2004; Andrut *et al.*, 2004). Fig. 1b displays the values of the structural relaxation coefficients obtained for the solid solutions, object of this study. As well depicted, ε can vary from 0 (no structural relaxation) to values that approach the hard sphere model.

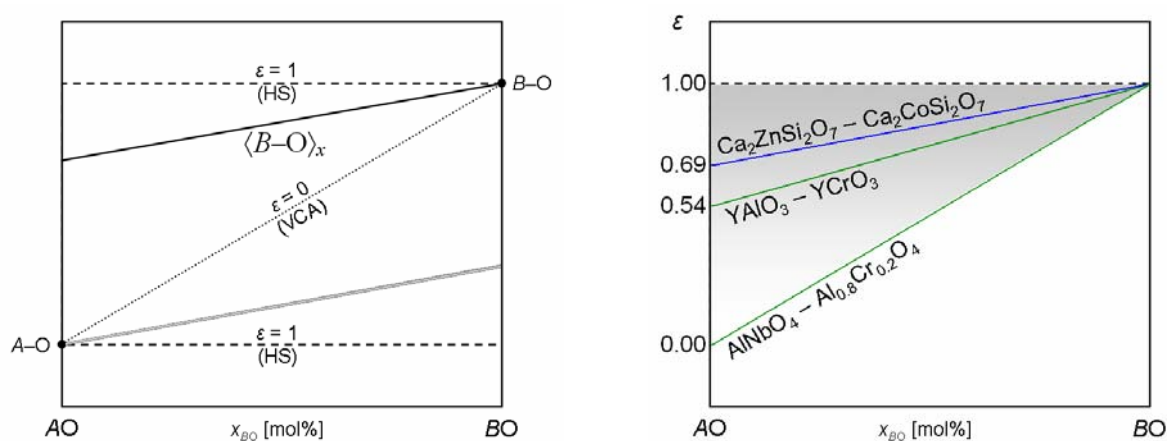


Fig. 1 - a) Dependence of the individual bond lengths in a binary solid solution $A_{1-x}B_xO$ according to different approaches. See text for explanation. Real changes of the individual local bond length, $\langle B-O \rangle_x$, is visualized by the black straight line between the VCA ($\varepsilon = 0$) and the HS ($\varepsilon = 1$) models. b) Graphical abstract of the structural relaxation coefficients (ε) obtained for the solid solution investigated in this work: $Y(Al_{1-x}Cr_x)O_3$ (refers to work A), $(Al_{1-x}Cr_x)NbO_4$ (refers to work C), $Ca_2(Zn_{1-x}Co_x)Si_2O_7$ (refers to work G).

Since the studies object of this work adopt the combined approach XRPD/EAS, here is briefly described the procedure used to achieve the structural relaxation coefficient for every solid solution reported afterward. The most common method to achieve the local metal–oxygen distances in a solid solution investigated through EAS is by means of the crystal field parameter $10Dq$, a measure of the length of a metal–oxygen bond related to the shift of the main optical bands of a transition metal ion (TMI) as a function of the amount of the TMI itself along a solid solution (e.g. Langer, 2001). According to the crystal field theory (Dunn, 1965; Burns, 1993), for the previously adopted hypothetical $AO-BO$ solid solution, the $10Dq$ value depends on the mean metal–oxygen bond distances by the relationship:

$$10Dq = 5/3 \cdot Q \cdot \langle r^4 \rangle \cdot \langle B-O \rangle^{-5} \quad (2)$$

where both the effective charge on the ligands Q and the average radius of d orbitals $\langle r \rangle$ can be considered constant for the same metal ion in the same ligand environment (Dunn, 1965; Marfunin, 1979; Burns, 1993;

Langer, 2001). The local metal–oxygen distance (*i.e.* $\langle B-O \rangle_x$) achieved by optical spectroscopy can be determined by means of previous equations as:

$$\langle B-O \rangle_x = \langle B-O \rangle_{x=1} \cdot [(10DqB)_{x=1} / (10DqB)_x]^{1/5} \quad (3)$$

Concluding, the so obtained latter value will lead to an easy calculation of the relaxation coefficient (ε) along the *AO–BO* solid solution by means of the Eq. 1.

EXPERIMENTAL SECTION

Synthesis procedures

The almost totality of the obtained compounds were synthesized *via* solid-state reaction, *i.e.* the conventional synthesis of ceramic powders (a: wet mixing and homogenization by ball milling in acetone of high purity raw materials; b: drying in oven at 100 °C; c: pulverization in agate mortar; d: pelletizing by using a piston cylinder press till ~ 80 MPa; e: calcination in alumina crucible using an electric kiln in static air, at a maximum temperature of 1200 °C for several hours and with a heating rate of 3 °C/min; f: natural cooling to room temperature). Just for the $YAlO_3$ – $YCrO_3$ perovskite solid solution a sol-gel combustion synthesis procedure was adopted (Blosi *et al.*, 2009).

X-ray powder diffraction and structural refinement strategies

XRPD data were collected at room temperature on a Bruker D8 Advanced diffractometer equipped with a Si(Li) solid-state detector, operating in the 5–130° 2 θ as maximum angular range, with a minimum scan rate of 0.015° 2 θ , and 10 s/step counting time.

The structural refinements were accomplished by the Rietveld method using the GSAS-EXPGUI software package. The presence of impurity phases (if any) was accounted for by carrying out multiphase refinements in which only the scale factors and the cell parameters were varied for the minor phases. Starting atomic models for the studied structure were taken from literature as indicated in Table 1. The refinements included cell parameters, atomic coordinates, isotropic atomic displacement parameters, a shifted Chebyshev polynomial to reproduce the background (the number of the coefficients varied from 15 to 18), zero-point, a scale factor (or phase fraction, in the case of samples with presence of impurity phases). The diffraction peak profiles were modeled by a pseudo-Voigt function.

Table 1 - Structure-type, stoichiometric formula, concentration of the substituting cations, and starting atomic model for each series of compounds investigated by means of X-ray powder diffraction. In the last column (reference to work) is indicated the label of the corresponding work described in “Result and Discussion”.

Structure-type (s.g.)	formula	x (apfu)	starting atomic model	ref. work
perovskite (s.g. <i>Pbnm</i>)	$Y(Al_{1-x}Cr_x)O_3$	0, 0.035, 0.075, 0.135, 0.25, 0.5, 0.75, 1	Cruciani <i>et al.</i> , 2005	A
alumoniobite (s.g. <i>C2/m</i>)	$(Al_{1-x}Cr_x)NbO_4$	0, 0.06, 0.125, 0.25, 0.375, 0.5	Greis <i>et al.</i> , 1996 Petersen & Müller-Buschbaum, 1992	C
melilite (s.g. <i>P-421m</i>)	$(Sr_{2-x}Ba_x)MgSi_2O_7$	0, 1, 1.5, 1.6, 1.75, 2	Kimata, 1983 Aitasalo <i>et al.</i> , 1996	D
melilite (s.g. <i>P-421m</i>)	$(x)_2(Mg_{0.7}Co_{0.3})Si_2O_7$	Ca, $Ca_{0.5}Sr_{0.5}$, Sr, $Sr_{0.5}Ba_{0.5}$, $Sr_{0.5}Ba_{1.5}$, $Sr_{0.25}Ba_{1.75}$	Kimata & Ii, 1981 Kimata, 1983 Aitasalo <i>et al.</i> , 1996	E
melilite (s.g. <i>P-421m</i>)	$Ca_2(Zn_{1-x}Co_x)Si_2O_7$	0, 0.25, 0.5, 0.75, 1	Bindi <i>et al.</i> , 2001	G
melilite (s.g. <i>P-421m</i>)	$Ca_2(Zn_{1-x}Co_x)Si_2O_7$	0.05, 0.1, 0.2, 0.3, 0.4	Bindi <i>et al.</i> , 2001	H
phenakite (<i>R-3H</i>)	$Zn_{2-x}Co_xSiO_4$	0, 0.05, 0.1, 0.2, 0.3	McMurdie <i>et al.</i> , 1986	L

UV-visible-NIR spectroscopy

EAS was performed by diffuse reflectance at room temperature by means of a Perkin Elmer spectrophotometer ($\lambda 19$ or $\lambda 35$) operating within 400-4000 nm range, 0.1 nm step size, with BaSO₄ integrating sphere, and BaSO₄ as white reference material. Reflectance (R) was converted to absorbance (K/S) by the Kubelka-Munk equation (Marfunin, 1979). Absorbance bands were deconvoluted by Gaussian function (*i.e.* the number of bands ranges from 7 to 13) starting from peak maxima by automatic fitting to convergence, in order to obtain band energy (centroid) and band width (FWHM).

In the case of Cr³⁺-doped compounds the crystal field strength $10Dq$ was calculated by fitting the energy of spin-allowed transitions in the d^3 Tanabe-Sugano diagram (Tanabe & Sugano, 1954; Andrut *et al.*, 2004) or simply taking the wavenumber of the ${}^4T_{2g}({}^4F)$ band = $10Dq$. Interelectronic repulsion Racah parameters were calculated as described in Lever (1984) and Wildner *et al.* (2004). The correspondent nephelauxetic ratios β_{35} and β_{55} (considered to express the covalent degree and polarizability of the Cr–O bonding, respectively) were calculated as $\beta = B/B_0$, where B is experimental and B_0 is the value of the free ion (Lever, 1984; Burns, 1993; Wildner *et al.*, 2004).

Similarly to the Cr³⁺ case, the crystal field strength $10Dq$ of Co²⁺-doped compounds (*i.e.* d^7 orbitals are involved) was calculated by fitting the energy of spin-allowed transitions in the d^3 Tanabe-Sugano diagram that is used, according to the d^{10-x} rule, in the case of ions in fourfold coordination (Tanabe & Sugano, 1954; Andrut *et al.*, 2004). In this case, it was not possible to determine directly the $10Dq$ value from the ${}^4T_{2g}({}^4F)$ band, as it is three-fold split and two of the three subbands fall out of the measured range. The effect of spin-orbit coupling, inducing a three-fold splitting of the spin-allowed transitions, was accounted by both averaging values of split bands and the baricenter method (Burns, 1993): the results so obtained differ for less than 0.5%.

RESULTS AND DISCUSSION

Premise

This chapter is organized in three sections. Each section provided a series of “key” studies developed under a common goal: to assess the relaxation coefficient ε around a doping *TMI* (*i.e.* Cr³⁺ and Co²⁺) hosted in different coordination site (*i.e.* octahedra and tetrahedra) along solid solutions of oxide and silicate structures. The survey methodology reflects that reported here in the “Introduction” and “Experimental Section”. Furthermore, in order to have a deeper and different perspective on the structural properties of the oxide and silicates investigated, other “satellite” works were also included. These latter works provided, for example, the high-pressure (HP) and the high-temperature (HT) behaviour of some of the end-members, or illustrated the technological performance of a solid solution, trying to provide, in that way, a comprehensive viewpoint of the investigated solid solutions.

The almost totality of the studied cases were published or submitted to peer-reviewed international scientific journals during the doctorate course. It will follow a brief abstract for each study that was more extensively developed throughout the dissertation. The corresponding references are given after each title; the letters k , s , and t within brackets stand for “key”, “satellite”, and “technological” study, respectively.

A - Structural relaxation around Cr³⁺ in YAlO₃-YCrO₃ perovskites from electronic absorption spectra. [k] Cruciani et al. (2009)

The structural relaxation around Cr³⁺ in YAl_{1-x}Cr_xO₃ perovskites was investigated and compared with analogous Cr–Al joins (corundum, spinel, garnet). Eight compositions (x_{Cr} from 0 to 1) were prepared by sol-gel combustion and were analyzed by a combined XRPD and EAS approach. The unit cell parameters and the XRPD averaged octahedral (Cr,Al)–O and ^[VIII]Y–O bond distances scale linearly with the chromium fraction. The optical parameters show an expected decrease of crystal field strength ($10Dq$) and an increase of covalency (B_{35}) and polarizability (B_{55}) towards YCrO₃, but a nonlinear trend outlines some excess $10Dq$ below $x_{Cr} \sim 0.4$. The local Cr–O bond lengths, as calculated from EAS, indicate a compression from 1.98 Å ($x_{Cr} = 1.0$) down to

1.95 Å ($x_{\text{Cr}} = 0.035$) so that the relaxation coefficient of perovskite ($\varepsilon = 0.54$) is the lowest in comparison with garnet ($\varepsilon = 0.74$), spinel ($\varepsilon = 0.68$) and corundum ($\varepsilon = 0.58$), in contrast with its structural features. The enhanced covalent character of the Cr–O–Cr bond in the one-dimensional arrangement of corner-sharing octahedra can be invoked as a factor limiting the perovskite polyhedral network flexibility. Increased probability of Cr–O–Cr clusters for x_{Cr} greater than ~ 0.4 is associated to diverging trends of nonequivalent interoctahedral angles bond. The relatively low relaxation degree of $\text{Y}(\text{Al,Cr})\text{O}_3$ can be also understood by considering an additional contribution to $10Dq$ because of the electrostatic potential of the rest of lattice ions upon the localized electrons of the CrO_6 octahedron. Such an “excess” $10Dq$ increases when the point symmetry of the Cr site is low, as in perovskite, and would be affected by the change of yttrium effective coordination number observed by XRPD for x_{Cr} greater than ~ 0.4 . This would justify the systematic underestimation of local Cr–O bond distances, as inferred from EAS, compared to what is derived from X-ray absorption (XAS) studies implying a stronger degree of relaxation around Cr^{3+} of all the structures considered and supporting the hypothesis that $10Dq$ from EAS contains more information than previously retained, particularly an additional contribution from the next nearest neighbouring ions.

B - Elastic properties of YCrO_3 up to 60 GPa. [s] Ardit et al. (2010)

The high pressure evolution of the YCrO_3 perovskite structure (space group $Pbnm$) has been investigated using synchrotron powder diffraction, up to 60 GPa. The results show an anisotropy in the elastic moduli of the individual crystallographic axes: the b axis is appreciably less compressible than both a and c axes [$K_{a0} = 195(5)$ GPa, $K_{b0} = 223(7)$ GPa, and $K_{c0} = 200(6)$ GPa, respectively]. This implies that YCrO_3 becomes more distorted with increasing pressure, which is similar to what was previously found in YTiO_3 but opposite to the behavior reported for YAlO_3 . Such contrasting trends are explained by the stronger confinement of Y ions in YAlO_3 due to the smaller size of octahedral network in the orthoaluminate compared to the orthochromate.

C - Structural stability, cation ordering, and local relaxation along the join $\text{AlNbO}_4\text{--Al}_{0.5}\text{Cr}_{0.5}\text{NbO}_4$. [k] Ardit et al. (2012a)

$(\text{Al}_{1-x}\text{Cr}_x)^{3+}\text{Nb}^{5+}\text{O}_4$ (with $0 \leq x \leq 0.5$) compounds have been investigated through combination of XRPD and EAS. In spite of the natural occurrence of AlTaO_4 , the lack of a mineral with composition AlNbO_4 contrasts with the strong geochemical affinity between Nb and Ta elements. Rietveld refinements of XRPD data showed that the effective coordination numbers of both the two non-equivalent octahedral sites ($M1$ and $M2$) in the AlNbO_4 structure are much lower than expected, especially the one mainly occupied by Nb, in agreement with the very low crystal field strength values ($10Dq$) found by EAS for Cr^{3+} replacing Al at site $M2$. These findings imply that an unfavorable bonding situation occurs for Nb, Al and Cr ions in the AlNbO_4 structure which can be regarded as substantially strained compared to AlTaO_4 , thus explaining the lack of a natural AlNbO_4 isomorph. The observed long local Cr–O distances (low $10Dq$) reveal that the AlNbO_4 lattice is not relaxed as a consequence of the Cr–Al substitution (the relaxation coefficient ε is close to zero) and the AlNbO_4 structure appears to follow the Vegard’s law. This is due to the fact that the Cr^{3+} for Al^{3+} substitution, for the limited range of solid solution (up to 0.2 apfu at site $M2$), does not induce any additional octahedral strain in a lattice already significantly strained.

D - Melilite-type and melilite-related compounds: structural variations along the join $\text{Sr}_{2-x}\text{Ba}_x\text{MgSi}_2\text{O}_7$ ($0 \leq x \leq 2$) and high-pressure behaviour of the two end-members. [s] Ardit et al. (2012b)

The structural variations along the solid solution $\text{Sr}_{2-x}\text{Ba}_x\text{MgSi}_2\text{O}_7$ ($0 \leq x \leq 2$), combined to the high pressure characterization of the two end-members, have been studied. A topological change from the tetragonal (melilite-type) to the monoclinic (melilite-related) structure along the join $\text{Sr}_2\text{MgSi}_2\text{O}_7$ (s.g. $P-42_1m$) – $\text{Ba}_2\text{MgSi}_2\text{O}_7$ (s.g. $C2/c$) occurs with a Ba content higher than 1.6 apfu. The tetragonal form, favored in the crystallization from a melt, has a tetrahedral sheet topology exclusively based on five-membered rings which provide a regular “4 up + 4 down” ligand arrangement. In contrast, the melilite-related structure, favored by solid-state reaction synthesis, is made by alternating six- and four-membered tetrahedral rings, that give an

asymmetric arrangement of alternated “5 up + 3 down” and “3 up + 5 down” ligands around Sr or Ba. This latter configuration is characterized by an additional degree of freedom with Ba polyhedra hosted in the interlayer with a more irregular and compact coordination and longer Ba–O bond distances. Further insights into the relationships between the two melilite typologies were achieved by investigating the *in situ* high pressure behavior of these systems. The synchrotron high-pressure experiments allowed to calculate the elastic moduli for the Sr melilite-type end-member and for the Ba monoclinic polymorph ($\text{Sr}_2\text{MgSi}_2\text{O}_7$: $K_{T0} = 107$, $K_{a=b} = 121$, and $K_c = 84$ GPa; $m\text{-Ba}_2\text{MgSi}_2\text{O}_7$: $K_{T0} = 85$, $K_a = 96$, $K_b = 72$, and $K_c = 117$ GPa) and compare them to those reported in the literature for åkermanite ($\text{Ca}_2\text{MgSi}_2\text{O}_7$). The results showed that, although the volume of Ba polyhedron in tetragonal polymorphs is larger than in the monoclinic forms, the interlayer compressibility is significantly lower in the former structures due to the occurrence of very short Ba–O distances. This unfavored Ba environment also makes tetragonal $\text{Ba}_2\text{MgSi}_2\text{O}_7$ a metastable phase at room conditions, possibly favored by high pressure. However, no phase transition occurs from monoclinic to tetragonal form due to kinetic hindrance in reconstructing the sheet topology.

E - Local structural investigation along the Ca–Sr–Ba-åkermanite solid solution doped with a fixed amount of tetrahedrally coordinated Co^{2+} . [k] Dondi et al. (2012)

In this study a first attempt to obtain information on the structural relaxation through a “probe cation” is proposed. The other cases of structural relaxation reported in this thesis, as well as in the literature, are founded on the calculation of the relaxation coefficient ε around an EAS-active cation, *i.e.* exhibiting electronic absorption transitions in the UV-visible-NIR spectrum (called “chromophore”). According to this approach, such a chromophore ion substitutes for the starting cation in the same polyhedron (octahedron or tetrahedron) and the structural relaxation is evaluated as a consequence of its increasing concentration. In the study here presented, on the other hand, the structural relaxation along the Ca–Sr–Ba-åkermanite solid solution (*i.e.* calculated around the eight-fold coordinated Sr^{2+} and Ba^{2+} , in the first and second part of the join, respectively) is achieved by evaluating the second shell effects of 0.3 mol of Co^{2+} (*i.e.* the “probe cation”) which replaces for Mg at T1 tetrahedral site. The chemical formulation of such a join, $(\text{Ca-Sr-Ba})_2(\text{Mg}_{0.7}\text{Co}_{0.3})\text{Si}_2\text{O}_7$, opens an original and roughly simple route to have local information by means of XRPD and EAS combined approach. Structural refinements of the XRPD data revealed a progressive lengthening of the mean polyhedral bond distances as a consequence of the lattice incorporation of cations progressively larger in the X cubic site, especially affecting the latter and, in a lesser manner, the T1 tetrahedral site. In agreement with the diffraction data, deconvolution of the optical spectra showed a progressive decreasing of the crystal field strength parameter $10Dq$ moving toward the Ba-åkermanite end-member. As a matter of fact, a linear correlation between mean and local cobalt–oxygen bond distance, $\langle \text{Mg}_{0.7}\text{Co}_{0.3}\text{-O} \rangle \propto \langle \text{Co-O} \rangle^{\text{local}}$, is observed. In order to evaluate the effect of the second next neighbours (Ca,Sr,Ba) on the T1 site, the increase of the tetrahedral distance found in an analogous undoped solid solution (see work D) was compared with the increase of the $\langle \text{Co-O} \rangle^{\text{local}}$ distance (as inferred from spectroscopic data obtained in this work). It was found that the $\langle \text{Co-O} \rangle^{\text{local}}$ distance increases slightly more than the $\langle \text{Mg-O} \rangle$ one. In other words, the melilite structure tends to relax more around Co^{2+} than Mg^{2+} once the T1 tetrahedron turns increasingly more distorted.

F - The inverse high temperature/high pressure relationship in the monoclinic $\text{Ba}_2\text{MgSi}_2\text{O}_7$ melilite-related structure. [s] Ardit et al. (2011)

High-temperature study of the synthetic melilite-related $\text{Ba}_2\text{MgSi}_2\text{O}_7$ (s.g. C2/c) was performed up to 1273 K. Linear thermal expansion coefficients along the unit cell edges and of the volume are $\alpha_a = 8.7 \times 10^{-6} \text{ K}^{-1}$, $\alpha_b = 11.0 \times 10^{-6} \text{ K}^{-1}$, $\alpha_c = 8.5 \times 10^{-6} \text{ K}^{-1}$, and $\alpha_V = 31.1 \times 10^{-6} \text{ K}^{-1}$, respectively, showing an anisotropic expansion behaviour characterized by $\alpha_a \approx \alpha_c < \alpha_b$. High-temperature data were then combined with high-pressure data (taken from the literature) for the same monoclinic sample. The “inverse relationship” of variation against temperature and pressure is observed for both the unit cell parameters and the (c/a) axial ratio as a function of the molar volume. A further comparison with melilite-type compound at ambient condition along the join

(Ca-Sr-Ba)₂MgSi₂O₇ reveals that the tetragonal polymorph of the barium compound (Ba₂MgSi₂O₇) should be a metastable phase favoured by high pressure conditions.

G - Local structural relaxation around Co²⁺ along the hardystonite–Co-åkermanite melilite solid solution. [k] Ardit et al. (2012c)

Six pure compounds belonging to the hardystonite (Ca₂ZnSi₂O₇) – Co-åkermanite (Ca₂CoSi₂O₇) solid solution were investigated by the combined application of XRPD and EAS. Structural refinements of the XRPD data revealed a negative excess volume of mixing due to the single isovalent substitution of Co for Zn in the tetrahedral site. In agreement with the diffraction data, deconvolution of the optical spectra showed a progressive decreasing of the crystal field strength parameter $10Dq$ moving toward the Co-aluminate end-member, meaning that the local cobalt–oxygen bond distance, $\langle\text{Co–O}\rangle^{\text{local}}$, increased along the join with the amount of cobalt. The calculated structural relaxation coefficient around the four-fold coordinated Co²⁺ in the Ca₂(Zn_{1-x}Co_x)Si₂O₇ join was $\varepsilon = 0.69$, very far from the one predicted by the Vegard's law ($\varepsilon = 0$), and at variance with $\varepsilon = 0.47$ previously found for tetrahedrally coordinated Co²⁺ in gahnite–Co-aluminate spinel solid solution. This difference is consistent with the largest constraints existing on the spinel structure, based on cubic closest packing, compared to the more flexible layered melilite structure.

H - Co-doped hardystonite, Ca₂(Zn,Co)Si₂O₇, a new blue ceramic pigment. [t] Dondi et al. (2011)

Raising cost, limited reserves, and toxicity make a pressing need to reduce the consumption of cobalt in the ceramic industry, trying to improve efficiency and sustainability of pigments. A novel blue colorant, based on the melilite structure, has been developed by searching for a ceramic pigment stable in very aggressive media, like the calcium- and zinc-rich glazes used in porous tiles (stoneware and monoporosa). Hardystonite was selected as a typical crystalline compound found in these coatings, which has just one four-fold crystallographic site where Co²⁺ ions can be accommodated, thus ensuring its unrivalled blue colour. Five samples (Ca₂Zn_{1-x}Co_xSi₂O₇ with $x = 0.05, 0.1, 0.2, 0.3$ and 0.4) were prepared by solid state synthesis in industrial-like conditions (~ 95% yield) and characterized by XRPD, DRS, SEM-EDS and technological testing. Increasing cobalt doping gives rise to a gradual expansion of the hardystonite unit cell, unexpected on the basis of Zn²⁺ and Co²⁺ ionic radii, attributed to a change of the covalent character of M–O bonding. Optical spectra are dominated by the strong absorption bands of Co²⁺ in tetrahedral coordination (crystal field strength $Dq = 421 \text{ cm}^{-1}$, Racah B parameter = 793 cm^{-1}). The best compromise between cobalt concentration and optical response was found to be around $x = 0.3$. The hardystonite pigment bestows a deep blue colour on glazes and glassy coatings, withstanding aggressive media rich in CaO and ZnO better than industrial blue pigments (cobalt aluminate, spinel) with similar colour efficiency than industrial blue dyes (cobalt silicate, olivine) but with the advantage to avoid specking defects of highly staining colorants.

I - Co-doped willemite ceramic pigments: technological behaviour, crystal structure and optical properties. [t] Ozel et al. (2010)

Cobalt-doped willemite is a promising blue ceramic pigment, but some important aspects concerning crystal structure, optical properties and technological behaviour are still undisclosed. In order to get new insight on these features, willemite pigments (Zn_{2-x}Co_xSiO₄, $0 < x < 0.3$) were synthesized by the ceramic route and characterized from the structural (XRPD with Rietveld refinement), optical (DRS and colorimetry), microstructural (SEM, STEM, TEM, EDX, EELS) and technological (simulation of the ceramic process) viewpoints. The incorporation of cobalt in the willemite lattice, taking preferentially place in the Zn1 tetrahedral site, induces an increase of unit cell parameters, metal-oxygen distances, and inter-tetrahedral tilting. It causes shifting and enhanced splitting of spin-allowed bands of Co²⁺ in tetrahedral coordination, implying slight changes of crystal field strength Dq and Racah B parameter, but increasing spin-orbit coupling parameter λ . Willemite pigments impart deep blue hue to ceramic glazes and glassy coatings with a colouring performance better than commercial Co-bearing colorants in the 800-1200 °C range. Detailed SEM-TEM investigation and

microanalysis proved that no diffusion phenomena occur at the pigment-glassy coating interface and that willemite pigments are chemically inert during firing at 1050 °C.

REFERENCES

- Aitasalo, T., Hölsä, J., Laamanen, T., Lastusaari, M., Letho, L., Niittykoski, J., Pellé, F. (2006): Crystal structure of the monoclinic $\text{Ba}_2\text{MgSi}_2\text{O}_7$ persistent luminescence material. *Z. Kristallogr. Suppl.*, **23**, 481-486.
- Andrut, M., Wildner, M., Rudiwicz, C. (2004): Optical absorption spectroscopy in geosciences. Part II: Quantitative aspects of crystal fields. In: "Spectroscopic methods in mineralogy", A. Beran & E. Libowitzky, eds. *EMU Notes in Mineralogy*, **6**, 145-188. Eötvös University Press, Budapest.
- Ardit, M., Dondi, M., Merlini, M., Bouvier, P., Cruciani, G. (2010): Elastic properties of YCrO_3 perovskite up to 60 GPa. *Phys. Rev. B*, **82**, 064109, 1-7.
- Ardit, M., Zanelli, C., Dondi, M., Cruciani, G. (2011): The inverse high temperature/high pressure relationship in the monoclinic $\text{Ba}_2\text{MgSi}_2\text{O}_7$ melilite-related structure. *Period. Mineral.*, **80**, 155-165.
- Ardit, M., Dondi, M., Cruciani, G. (2012a): Structural stability, cation ordering, and local relaxation along the AlNbO_4 - $\text{Al}_{0.5}\text{Cr}_{0.5}\text{NbO}_4$ join. *Am. Mineral.*, **97**, 910-917.
- Ardit, M., Dondi, M., Merlini, M., Cruciani, G. (2012b): Melilite-type and melilite-related compounds: structural variations along the join $\text{Sr}_{2-x}\text{Ba}_x\text{MgSi}_2\text{O}_7$ ($0 \leq x \leq 2$) and high-pressure behaviour of the two end-members. *Phys. Chem. Minerals*, **39**, 199-211.
- Ardit, M., Cruciani, G., Dondi, M. (2012c): Local structural relaxation around Co^{2+} along the hardystonite–Co-åkermanite melilite solid solution. *Phys. Chem. Minerals*, Under revision.
- Bindi, L., Czank, M., Röthlisberger, F., Bonazzi, P. (2001): Hardystonite from Franklin furnace: a natural modulated melilite. *Am. Mineral.*, **86**, 747-751.
- Blosi, M., Albonetti, S., Costa, A., Dondi, M., Ardit, M., Cruciani, G. (2009): Sol-gel combustion synthesis of chromium doped yttrium aluminum perovskites. *J. Sol-Gel Sci. Technol.*, **50**, 449-455.
- Burns, R. (1993): Mineralogical applications of crystal field theory, 2nd edition. Cambridge University Press, Cambridge. 551 p.
- Cruciani, G., Matteucci, F., Dondi, M., Baldi, G., Barzanti, A. (2005): Structural variations of Cr-doped (Y,REE)AlO₃ perovskites. *Z. Kristallogr.*, **220**, 930-937.
- Cruciani, G., Ardit, M., Dondi, M., Matteucci, F., Blosi, M., Dalconi, M.C., Albonetti, S. (2009): Structural relaxation around Cr^{3+} in YAlO_3 - YCrO_3 perovskites from electron absorption spectra. *J. Phys. Chem. A*, **113**, 13772-13778.
- Dondi, M., Zanelli, C., Ardit, M., Cruciani, G. (2011): Co-doped hardystonite, $\text{Ca}_2(\text{Zn},\text{Co})\text{Si}_2\text{O}_7$, a new blue ceramic pigment. *J. Am. Ceram. Soc.*, **94**, 1025-1030.
- Dondi, M., Ardit, M., Cruciani, G. (2012): Local structural investigation along the Ca-Sr-Ba-åkermanite solid solution doped with a fixed amount of tetrahedrally coordinated Co^{2+} . *Chem. Mater.*; in prep.
- Dunn, T., McClure, D., Pearson, R. (1965): Some aspects of crystal field theory. Harper and Row eds., New York. 115 p.
- Galoisy, L. (1996): Local versus average structure around cations in minerals from spectroscopic and diffraction measurements. *Phys. Chem. Minerals*, **23**, 217-225.
- Geiger, C. (2001): Solid solutions: Background, history and scientific perspective. In: "Solid solutions in silicate and oxide systems", C. Geiger, Ed. *EMU Notes in Mineralogy*, **3**, 3-7. Eötvös University Press, Budapest.
- Greis, O., Ziel, R., Garcia, D., Claussen, N., Breidenstein, B., Haase, A. (1996): Crystal structure and morphology of disordered AlNbO_4 from X-ray powder diffraction. *Mat. Sci. Forum*, **228**, 825-830.
- Kimata, M. (1983): The structural properties of synthetic Sr-åkermanite, $\text{Sr}_2\text{MgSi}_2\text{O}_7$. *Z. Kristallogr.*, **163**, 295-304.
- Kimata, M. & Ii, N. (1981): The crystal structure of synthetic åkermanite, $\text{Ca}_2\text{MgSi}_2\text{O}_7$. *N. Jb. Miner. Monat.*, 1-10.
- Langer, K. (2001): A note on mean distances, $R_{[\text{MO}_6]}$, in substituted polyhedra, $[(\text{M}_{1-x}\text{M}_x)\text{O}_6]$, in the crystal structures of oxygen based solid solutions: local versus crystal averaging methods. *Z. Kristallogr.*, **216**, 87-91.
- Lever, A. (1984): Inorganic electronic spectroscopy, 2nd edition. Elsevier, Amsterdam. 864 p.
- Marfunin, A.S. (1979): Physics of minerals and inorganic materials. Springer, Berlin-Heidelberg-New York. 340 p.
- McMurdie, H., Morris, M., Evans, E., Paretzkin, B., Wong-Ng, W., Hubbard, C. (1986): Standard X-ray diffraction powder patterns from the JCPDS research associationship. *Powder Diffr.*, **1**, 265-275.
- Mikkelsen, J.K. & Boyce, J.B. (1983): Extended X-ray-absorption fine-structure study of $\text{Ga}_{1-x}\text{In}_x\text{As}$ random solid solutions. *Phys. Rev. B*, **28**, 7130-7140.
- Ozel, E., Yurdakul, M., Turan, S., Ardit, M., Cruciani, G., Dondi, M. (2010): Co-doped willemite ceramic pigments: Technological behaviour, crystal structure and optical properties. *J. Eur. Ceram. Soc.*, **30**, 3319-3329.
- Petersen, A. & Müller-Buschbaum, H. (1992): Ein Beitrag über Oxide vom Typ AMO_4 (A= Ti^{3+} , Cr^{3+} ; M= Nb^{5+} , Ta^{5+}). *Z. Anorg. Allg. Chem.*, **609**, 51-54.

- Tanabe, Y. & Sugano, S. (1954): On the absorption spectra of complex ions. I and II. *J. Phys. Soc. Jpn.*, **9**, 753-779.
- Urusov, V. (1992): A geometric model of deviations from Vegard's rule. *J. Solid State Chem.*, **98**, 223-236.
- Urusov, V. (2001): The phenomenological theory of solid solutions. In: "Solid solutions in silicate and oxide systems", C. Geiger, Ed. *EMU Notes in Mineralogy*, **3**, 121-153. Eötvös University Press, Budapest.
- Vegard, L. (1921): Die Konstitution der Mischkristalle und die Raumfüllung der Atome. *Z. Phys.*, **5**, 17-26.
- Wildner, M., Andrut, M., Rudowicz, C. (2004): Optical absorption spectroscopy in geosciences. Part I: Basic concepts of crystal field theory. In: "Spectroscopic methods in mineralogy", A. Beran & E. Libowitzky, eds. *EMU Notes in Mineralogy*, **6**, 93-140. Eötvös University Press, Budapest.